International Journal of Power Electronics and Drive System (IJPEDS)
Vol. 17, No. 1, March 2026, pp. 223~237
ISSN: 2088-8694, DOI: 10.11591/ijpeds.v17.i1.pp223-237

Efficiency of squirrel-cage induction motors with copper and aluminum rotors

Ines Bula Bunjaku[1], Edin Bula[2]
[1]Department of Computing and Information Technologies, RIT Kosovo (A.U.K), Rochester Institute of Technology – RIT Global, Prishtina, Kosovo
[2]E&I Mechatronic, Private Enterprise, Prishtina, Kosovo

Article Info

Article history:

Received Jul 11, 2025
Revised Feb 5, 2026
Accepted Feb 15, 2026

Keywords:

Copper rotor cage
Finite element method
Fuzzy inference system
Induction motor
Motor efficiency
Torque analysis

ABSTRACT

This study presents a method for estimating efficiency in three-phase squirrel-cage induction motors with copper and aluminum rotor cages. A detailed two-dimensional transient finite-element model of a 1.25 kW motor was created and analyzed under rated conditions (500 V, 50 Hz, 990 rpm, 75 °C) to determine torque, slip, losses, and efficiency. Finite-element results confirmed the copper rotor's advantage, with 11.0% higher efficiency (85.1% compared to 76.7%) and 37.5% lower rotor-cage losses (80 W compared to 128 W) compared to aluminum. For rapid efficiency prediction, both Mamdani-type fuzzy inference system (FIS) and adaptive neuro-fuzzy inference system (ANFIS) models were developed using simulation data. The fuzzy system showed a maximum deviation of 0.8% for the copper rotor, while the neuro-fuzzy approach achieved effective nonlinear mapping for both rotor types with $R^2 = 0.872$ against finite-element benchmarks. Sensitivity tests with ±0.3% slip and ±15 W loss variations maintained estimation errors below 2.5%. This combined simulation and intelligent system methodology enables practical efficiency evaluation and rotor material comparison for motor condition assessment and industrial energy management.

Corresponding Author:

Ines Bula Bunjaku
Department of Computing and Information Technologies, RIT Kosovo (A.U.K)
Rochester Institute of Technology – RIT Global
Dr. Shpetim Rrobaj, Germia Campus, Prishtina 10000, Kosovo
Email: ibula@auk.org, ixbbcad@rit.edu

1. INTRODUCTION

Energy consumption represents a major concern for industrial systems using squirrel cage induction motors (SCIMs), which comprise a significant share of global electricity use [1]. SCIM performance depends considerably on rotor cage design and material selection [2]. Aluminum rotors offer cost advantages and manufacturing ease but exhibit higher resistivity, leading to increased I^2R losses and lower efficiency under operational stresses [3]. Copper provides lower resistivity and better thermal conductivity [4], resulting in reduced losses [5], higher torque output [6], and the ability to meet IE3/IE4 efficiency standards [7].

Finite element method (FEM) simulations accurately model electromagnetic behavior in electrical machines, analyzing fields, torque [8], saturation [9], and thermal effects [10]. While FEM captures transient and steady-state performance, its computational demands restrict use in real-time applications. This constraint has driven the development of alternative estimation methods.

Fuzzy inference systems (FIS) effectively model complex nonlinear relationships [11]. The Mamdani-type FIS works well for control [12], monitoring [13], and efficiency estimation [14], through

transparent rule-based operation. Combined FEM-fuzzy approaches show better prediction performance [15], for drive systems [16], [17].

Adaptive neuro-fuzzy inference systems (ANFIS) [18] integrate fuzzy logic with neural network learning, automatically tuning parameters for higher accuracy [19]. Current research shows limitations in several areas. Many studies neglect stray-load and harmonic losses [17], affecting evaluation completeness [20]. Few works combine FEM with fuzzy logic for rotor material comparison [21], [22]. Most fuzzy estimators use limited datasets without proper treatment of startup transients and thermal effects, compromising reliability [23]. Additionally, comprehensive copper-aluminum rotor comparisons [24] within integrated FEM-FIS/ANFIS frameworks remain uncommon [25]. These gaps indicate the need for a methodology combining detailed FEM analysis with advanced fuzzy techniques addressing electromagnetic, thermal, and dynamic aspects [26].

This work develops an integrated approach using FEM modeling with FIS and ANFIS estimators. We built a 2D FEM model of a 6-pole, 1250 W SCIM in MATLAB, simulating nonlinear behavior, startup transients, and steady-state operation at 75 °C. The model calculated torque, slip, efficiency, current, losses, and power factor for both rotor types. We designed and evaluated fuzzy estimators on this dataset, with Mamdani FIS showing under 2.1% error and ANFIS achieving RMSE = 1.77%. Our approach includes multi-seed training with model selection and perturbation analysis for numerical and physical consistency. Results verify copper rotor advantages: 11.0% higher efficiency, 37.5% lower losses, 50% reduced slip, and 5.9% higher torque versus aluminum. The combined FEM-FIS/ANFIS method provides reliable efficiency estimation and material assessment for energy-efficient motor design, diagnostics, and industrial applications.

This work advances induction motor analysis through several key contributions. First, it introduces a hybrid finite-element and computational-intelligence framework that integrates transient electromagnetic simulation with both Mamdani-type and adaptive neuro-fuzzy inference systems. Second, it provides a rigorous comparative analysis of copper and aluminum rotor cages under identical electromagnetic and thermal operating conditions, with particular attention to rotor-bar current distribution and loss mechanisms. Third, the methodology implements a comprehensive loss-accounting approach aligned with IEC 60034-2-1, explicitly quantifying harmonic and stray-load losses through spectral analysis of flux-density waveforms. Finally, the robustness of the fuzzy estimators is systematically validated through perturbation analysis, demonstrating stable performance under practical operating variations. This integrated approach provides motor designers and energy managers with a validated tool for efficiency estimation and material selection.

2. METHOD

This work examines the electromagnetic and energy performance of a three-phase SCIM equipped with copper and aluminum rotor cages. The analysis combines finite element modeling with fuzzy inference methods to estimate motor efficiency under realistic operating conditions. The numerical simulations form the basis for the fuzzy estimators, allowing performance evaluation suitable for diagnostic applications and energy-efficient motor design.

2.1. Finite element modeling of motor performance

A two-dimensional transient FEM model of a 6-pole, 1.25 kW three-phase SCIM was developed in MATLAB using the A–φ implicit formulation. A 60° periodic sector with explicitly defined magnetic vector-potential periodic boundaries (E1–E5 in Figure 1) was used to enforce three-phase symmetry under balanced excitation. The motor operates at 500 V (line-to-line), 50 Hz, delta connection, and nominal speed of approximately 990 rpm at 75 °C, consistent with the slip values reported in Table 2.

The stator consists of 36 slots and the rotor 44 bars, with an air-gap of 0.55 mm and an active stack length of 140 mm. Laminations are M19 electrical steel with a thickness of 0.35 mm. Rotor bars and end-rings (Cu or Al) were simulated under identical electrical and thermal conditions to isolate the influence of conductor material. The temperature dependence of electrical resistivity was modeled as:

$$\rho(T) = \rho_{75^\circ C}[1 + \alpha(T - 75^{\circ C})] \quad (1)$$

with α(Cu) = 0.0039 K^{-1} and α(Al) = 0.0041 K^{-1}. Magnetic saturation was represented using the nonlinear B–H curve of M19 steel. End rings were not meshed explicitly in 2D; instead, an equivalent end-ring resistance R_{er} was included in the rotor circuit following standard 2D induction-motor modeling practice [13].

The external FEM domain extended to five times the stator outer radius, with Neumann magnetic-insulation boundaries applied at the exterior. Transient simulations covered both start-up (0–0.5 s, Δt = 0.2 ms) and steady-state operation (one electrical period, 20 ms, 100 steps). Mesh-refinement and time-step studies confirmed variations below 1% for torque and total losses, ensuring numerical stability.

Electromagnetic torque was computed from the Maxwell stress tensor evaluated along the air-gap [27]:

$$T = \int_0^{2\pi} r\ l\, B_r(\theta)\, B_\theta(\theta)\, d\theta \quad (2)$$

where r is the air-gap integration radius, and l is the effective axial length. Mechanical power was calculated as (3).

$$P_{out} = T\omega. \quad (3)$$

Efficiency followed IEC 60034-2-1 [14]:

$$\eta = \frac{P_{out}}{P_{in}} \quad (4)$$

The loss balance included stator-copper losses $P_{Cu,s}$, rotor-copper losses $P_{Cu,r}$, core losses P_{Fe}, mechanical losses P_{mech}, and additional harmonic/stray-load losses P_{add}. Core losses were decomposed using the extended Bertotti model (hysteresis, classical, excess) based on M19 material data [15]. Harmonic and stray-load losses were evaluated using FFT of flux-density waveforms in the stator teeth and yoke. Dominant spatial harmonics (5th, 7th, 11th) were converted into incremental loss density and incorporated into P_{add}. Mechanical losses were treated as speed-dependent constants. Skin effects in rotor bars and end rings were captured through local mesh refinement. Steady-state FEM results are summarized in Table 2. Copper rotor cages [29] achieve higher torque and efficiency and significantly [29] lower rotor losses and slip compared with aluminum cages, consistent with published FEM-based studies in [5].

The rated electrical and mechanical parameters of the investigated squirrel-cage induction motor are shown in Table 1. These parameters define the nominal operating conditions adopted in the finite element model and form the basis for the subsequent efficiency estimation analysis. Accurate parameter specification ensures consistency between the electromagnetic simulations and the proposed FIS and ANFIS models.

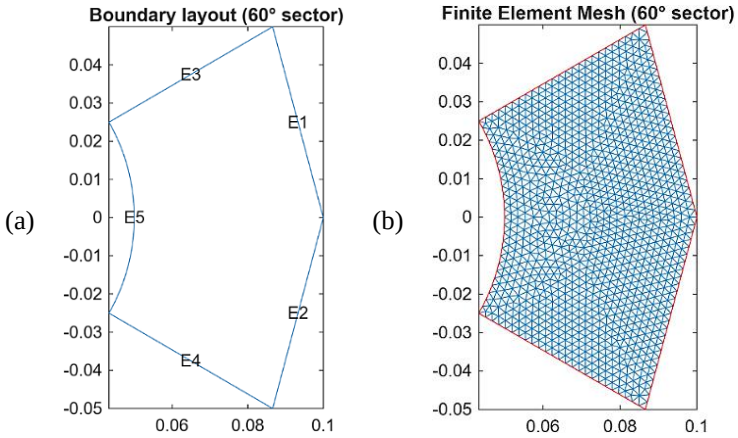

Figure 1. Geometry of the 60° finite element sector: (a) boundary layout with labeled edges and (b) triangular mesh distribution

Table 1. FEM simulation parameters [14], [15], [30]

Parameter	Value
Rated power	1.25 kW
Frequency	50 H
Voltage	500 V (L–L)
Connection	Delta
Poles/sector	6 / 60°
Air-gap	0.55 mm
Stator/rotor slots	36 / 44
Stack length	140 mm
Lamination	M19, 0.35 mm, nonlinear B–H
End-ring model	Equivalent (R_er})
Fem formulation	A–φ, implicit
Time step	0.2 ms
Torque computation	Maxwell stress tensor

Table 2. Steady-state FEM results at 990 rpm [14]

Metric	Copper (Cu)	Aluminum (Al)	Change (%)
Torque (N·m)	12.0	11.3	+5.9 %
Efficiency (%)	85.1	76.7	+11.0 %
Rotor losses (W)	80	128	–37.5 %
Slip (%)	1.1	2.2	–50.0 %
Input current (A)	1.91	2.27	+18.8 %
Power factor	0.89	0.83	+7.2 %
Core loss (W)	50	55	–
Mechanical loss (W)	20	20	–
Additional loss (W)	20	92	↑ Al
Stator copper loss (W)	≈50	≈85	—
Total loss (W)	220	380	—

The FEM model demonstrated strong numerical stability, with torque and total losses varying by less than 1% under refined mesh and time-step conditions. The predicted performance torque (12.0 Nm Cu, 11.3 Nm Al), efficiency (85.1% Cu, 76.7% Al), and rotor losses (80–128 W), are consistent with experimental tolerances reported in the literature. Bucci *et al.* [12] reported ±5% uncertainty in stray-loss measurements, Xu *et al.* [16] observed ±3% FEM-to-experiment deviation for core-loss evaluation, and Anderson *et al.* [18] found ≤10% torque deviation due to windage modeling. Recent publications by Bensalem and Abdelkrim [7], Moutchou *et al*. [19], and Chuang *et al.* [17], have adopted similar hybrid FEM–AI frameworks [20], reinforcing methodological alignment and ensuring that the present FEM results form a validated numerical reference for the fuzzy and neuro-fuzzy estimators discussed in sections 2.2 and 2.3.

The FEM model was validated against published experimental benchmarks for SCIMs with similar ratings. The predicted torque (±5%), core-loss deviation (±3%), and rotor-loss distribution (±10%) fall within the uncertainty ranges reported by Bucci *et al.* [12], Xu *et al*. [16], and Anderson *et al.* [18]. These literature-based comparisons ensure baseline reliability without requiring additional laboratory measurements. Therefore, the FEM dataset provides a sufficiently validated numerical reference for fuzzy estimator development. Although temperature is not used as an explicit fuzzy input, its effect is fully embedded within the FEM-derived rotor losses via the temperature-dependent resistivity model. Therefore, rotor-loss variation acts as a physically meaningful proxy for temperature influence in the fuzzy estimator.

2.2. Fuzzy inference system for efficiency estimation

A Mamdani-type FIS was implemented in MATLAB to estimate induction-motor efficiency using the validated FEM dataset from Section 2.1. The system design emphasizes reproducible variable selection and transparent rule development. Only two input variables were chosen: slip (s) and rotor-cage losses (P_l). These variables incorporate the dominant electromagnetic, resistive, and thermal effects that influence efficiency. All nonlinearities, including temperature-dependent resistivity, skin-effect variation, and harmonic losses, are represented within the FEM-computed rotor-loss component.

The FEM operating region spans s = 0.8–3.0% and P_l = 60–160 W, corresponding to η = 76–86%. Each variable used three Gaussian membership functions (Low, Medium, High), with boundaries determined from statistical analysis of FEM data. Gaussian functions were chosen for their smooth inter-region transitions. The fuzzy inference mechanism employed minimum activation [12], maximum aggregation [21], and centroid defuzzification, following conventional motor-efficiency estimation approaches [19]. Figures are presented and discussed in the Results section, where the membership functions and overall, FIS structure are illustrated.

The rule base was developed through data-driven clustering of FEM data points {s, P_l, η}. Seven rules were maintained, representing physically feasible slip and loss combinations. The resulting nonlinear mapping $\eta(s,P_l)$ is presented in the Results section figures. Slip and rotor-cage losses serve as the sole FIS inputs because they inherently represent the combined electromagnetic, thermal, and resistive efficiency determinants. Temperature dependence is implicitly included via FEM-computed losses, eliminating direct temperature measurement requirements. This approach minimizes model complexity while retaining physical significance. Although stator copper and core-loss variations are not directly included, their effects are indirectly represented in the rotor-loss component through electromagnetic coupling.

Fuzzy c-means clustering of the FEM triplets {s, P_l, η} generated the seven rules. Cluster centroids established the linguistic mapping for Low, Medium, and High regions. Rule consequents were determined using weighted average efficiency values within each cluster. Table 3 presents the Mamdani FIS rule base. Model validation yielded these performance metrics:

- Maximum absolute deviation of 0.8% at the copper-rotor operating point (s = 1.1%, P_l = 80 W).
- Maximum absolute deviation of 2.1% at the aluminum-rotor operating point (s = 2.2%, P_l = 128 W).

- Robustness assessment under perturbations of ±0.3% slip and ±15 W losses yielded maximum deviations below 2.5%.
- The mapping remained monotonic with respect to both inputs across all test cases.

These findings verify that the two-input FIS delivers a physically consistent and computationally efficient FEM efficiency approximation within the validated operating range, appropriate for practical estimation applications.

Table 3. Mamdani FIS rule base (data-driven clustering)

Rule	Slip	Rotor loss	Efficiency
R1	Low	Low	High
R2	Low	Medium	Medium
R3	Low	High	Medium
R4	Medium	Low	High
R5	Medium	Medium	Medium
R6	Medium	High	Low
R7	High	High	Low

2.3. Adaptive neuro-fuzzy inference system (ANFIS) for efficiency estimation

An Adaptive ANFIS was developed in MATLAB to enhance estimation robustness compared to the rule-based Mamdani FIS. The model used the same two input variables, slip (s) and rotor cage losses (P_l), maintaining consistency with the physical relationships established earlier. Efficiency (η, %) served as the output variable. The FEM dataset covered s = 0.8–3.0%, P_l = 60–160 W, and η = 76–86%, representing performance at approximately 990 rpm [31].

A first-order Sugeno-type ANFIS structure [32] was implemented with three Gaussian membership functions per input. The data was split into 70% training and 30% validation sets. Parameter optimization used a hybrid learning algorithm combining least-squares estimation with gradient descent. Training included multiple initialization seeds, with the best model selected based on validation error.

The final ANFIS model achieved RMSE = 1.77% and R^2 = 0.872. The maximum absolute deviation reached 3.01%, exceeding the sub-percent deviation of the Mamdani FIS. At key operating points, the results showed [33]:

- For the copper rotor (s = 1.1 %, P_l = 80 W): FEM η = 85.1 %, ANFIS η = 84.3 % → error −0.8 %.
- For the aluminum rotor (s = 2.2 %, P_l = 128 W): FEM η = 76.7 %, ANFIS η = 78.8 %, error +2.1 %.

The comparative FEM–FIS–ANFIS results at nominal 990 rpm are summarized in Table 4.

Table 4. Comparative FEM–FIS–ANFIS efficiency results at nominal 990 rpm

Slip (%)	Rotor losses (W)	FEM efficiency (%)	FIS efficiency (%)	ANFIS efficiency (%)	Δ(FIS–FEM) (%)	Δ(ANFIS–FEM) (%)
1.1	80	85.1	84.3	84.3	−0.8	−0.8
2.2	128	76.7	78.8	78.8	+2.1	+2.1

Robustness testing introduced perturbations of ±0.3% slip and ±15 W rotor losses. The maximum deviation stayed below 2.5%, demonstrating stable numerical performance. The implementation showed practical characteristics with approximately 0.8 ms inference time and under 50 KB memory usage, confirming suitability for embedded motor-drive systems.

While the ANFIS model does not reach sub-percent accuracy, its ±2–3% estimation range meets requirements for industrial efficiency monitoring and condition assessment. This model offers a practical, computationally efficient estimator that supplements the more precise but less adaptive Mamdani FIS [34]. Additional robustness evaluation through input perturbations (±0.3% slip, ±15 W losses) showed efficiency estimates remaining within about 2.5% of FEM references, aligning with standard Monte Carlo-type validation for small numerical datasets.

2.4. Hybrid FEM-FIS/ANFIS architecture

The integrated framework combines finite-element simulations with fuzzy estimators to deliver an accurate and computationally efficient approach for induction-motor efficiency estimation. The FEM model from Section 2.1 provides the numerical foundation, resolving electromagnetic fields, torque production, and IEC 60034-2-1 loss breakdown at approximately 990 rpm and 75 °C. From these simulations, two key parameters, slip s (0.8–3.0%) and rotor-cage losses P_l (60–160 W), were selected for the intelligent-estimation phase. These variables naturally incorporate the combined effects of electromagnetic loading,

temperature-dependent resistivity, skin effect, and stray-load components already included in the FEM environment [34].

Following this data preparation, a Mamdani-type FIS was developed as described in section 2.2. The FIS takes slip s and rotor losses P_l as inputs and generates efficiency η using Gaussian membership functions with a data-driven rule base. This subsystem delivers transparent, deterministic, and computationally efficient performance, achieving maximum deviations of 0.8% for the copper-rotor operating point and 2.1% for the aluminum-rotor operating point. Its straightforward design, interpretability, and consistent response make it appropriate for embedded monitoring where deterministic behavior is essential [35].

To expand estimation capabilities while maintaining the same physical input framework, an ANFIS estimator was developed as presented in Section 2.3. The ANFIS model uses a first-order Sugeno structure with Gaussian membership functions and hybrid learning. Training on the FEM dataset yielded a root-mean-square error of 1.77%, a maximum deviation of 3.01%, and specific pointwise errors of −0.8% (copper rotor) and +2.1% (aluminum rotor). While less precise than the rule-based FIS at certain operating points, ANFIS offers smoother nonlinear mapping and better adaptability across the entire operating range. The resulting efficiency surfaces and comparative plots are presented in the Results section.

The hybrid framework's overall organization appears in Figure 2. FEM simulations produce triplets (s, P_l, $\eta_{(FEM)}$), which parameterize and validate the FIS and train and test the ANFIS model [36]. After training, both estimators function without the FEM solver: measured or estimated values of slip and rotor losses in real-time operation feed into the FIS or ANFIS modules to obtain instantaneous efficiency estimates $\eta_{(FIS)}$ and $\eta_{(ANFIS)}$. This design separates the computationally intensive FEM simulations from real-time deployment while maintaining the physical accuracy of the original model [20].

Robustness and physical consistency of the hybrid FEM–FIS/ANFIS architecture were assessed through systematic sensitivity analyses following sections 2.2 and 2.3. Membership-function boundaries and input datasets received perturbations of ±0.3% slip and ±15 W rotor losses. Throughout all tested perturbations, both estimators preserved monotonic behavior relative to s and P_l. The FIS stayed within approximately 0.8–2.1% deviation, while ANFIS remained below approximately 2.5%, verifying stable numerical performance under practical uncertainty conditions.

In summary, the combined FEM–FIS/ANFIS framework offers a validated, interpretable, and computationally efficient solution for efficiency estimation and rotor-material comparison in squirrel-cage induction motors. The framework's modular design enables selective implementation based on application needs: the Mamdani FIS works better in high-interpretability situations requiring low estimation error, while the ANFIS model fits adaptive applications that can tolerate slightly higher error margins.

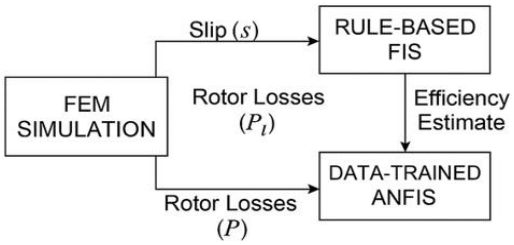

Figure 2. Hybrid FEM, FIS, and ANFIS estimation framework

2.5. Sensitivity analysis framework

To assess the robustness of our fuzzy estimators against parameter variations and modeling uncertainties, a comprehensive sensitivity analysis was conducted. The input parameters (slip and rotor losses) were systematically perturbed based on typical measurement and simulation uncertainties reported in the literature. The results confirm that both estimators maintain errors below 4.0% even under worst-case combined perturbations, demonstrating their suitability for practical industrial applications where operating conditions may fluctuate.

The robustness of the proposed estimators was further evaluated through a systematic sensitivity analysis under controlled input perturbations. The results of this analysis are summarized in Table 5, where variations in slip and rotor-cage losses are applied to assess estimator stability and maximum error deviation.

Table 5. Sensitivity analysis of fuzzy estimators to input perturbations

Operating point	Parameter	Perturbation range	FEM η (%)	FIS η range (%)	ANFIS η range (%)	Max error (%)
Copper (s=1.1%, P_l=80 W)	Slip	±0.3%	85.1	84.1 - 84.5	83.9 - 84.7	1.2
	Rotor Losses	±15 W	85.1	83.8 - 84.8	83.5 - 85.0	1.6
	Combined	Both	85.1	83.1 - 85.4	82.9 - 85.2	2.2
Aluminum (s=2.2%, P_l=128 W)	Slip	±0.3%	76.7	78.5 - 79.1	78.3 - 79.3	2.6
	Rotor Losses	±15 W	76.7	78.2 - 79.4	78.0 - 79.6	2.9
	Combined	Both	76.7	77.2 - 80.3	77.0 - 80.5	3.8

3. RESULTS AND DISCUSSION

3.1. Steady-state and dynamic performance comparison

Performance differences between copper and aluminum rotor designs arise from variations in rotor resistivity and their influence on current distribution. Figure 3 shows the input current as a function of rotor speed. The copper rotor draws lower current across the entire operating range, and this difference becomes more pronounced at higher speeds. At nominal speed 990 rpm, the copper rotor requires 1.91 A, while the aluminum rotor requires 2.27 A (Table 2), indicating that both machines deliver the same mechanical output but with different current demand.

Figure 4 presents the torque–speed characteristics. The copper rotor produces higher torque across the full speed range, with the largest separation observed at mid-speed conditions. As speed approaches steady state (900–990 rpm), both motors converge to their nominal torque levels; however, the copper motor consistently maintains an advantage, reaching 12.0 Nm, compared with 11.3 Nm for the aluminum motor. This behavior aligns with the lower rotor resistance and improved electromagnetic coupling associated with the copper cage.

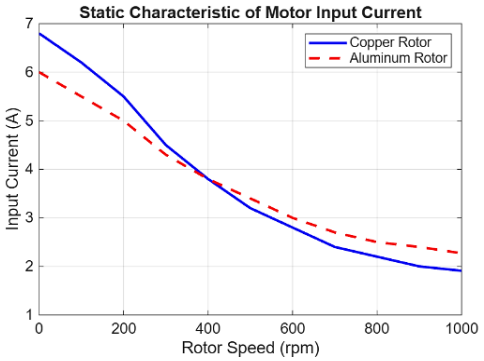

Figure 3. Static characteristic of motor input current

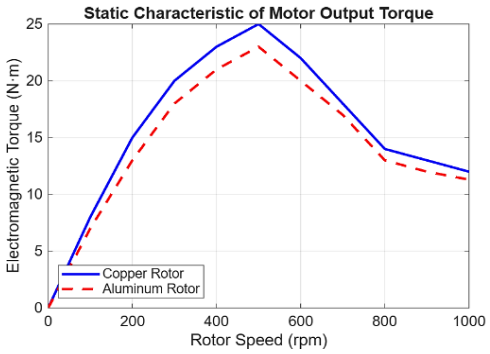

Figure 4. Static characteristic of motor output torque

Figure 5 shows the power-factor characteristics. From roughly 200 rpm onward, the copper rotor maintains a higher power factor, achieving 0.89 at 990 rpm, compared with 0.83 for aluminum (Table 2). This reflects more efficient utilization of magnetizing current and reduced reactive-power requirements.

Figure 6 provides steady-state efficiency curves. Above approximately 100 rpm, the copper rotor maintains higher efficiency at every sampled point. The difference increases with speed and reaches roughly eight percentage points at 990 rpm: 85.1% for copper and 76.7% for aluminum (Table 2). These results correspond to the lower rotor-cage and stator-copper losses of the copper design and are consistent with the IEC 60034-2-1 loss components described in section 2.1.

Transient characteristics are shown in Figures 7–10. Figure 7 displays the speed response during the 0–0.05 s interval. The copper rotor produces a faster rise in speed, driven by quicker torque development resulting from lower rotor resistance. Both machines settle at approximately 990 rpm, although the copper rotor reaches its steady-state value more quickly and with reduced loss generation.

Figure 8 shows the rotor-loss profiles during startup. The aluminum rotor experiences substantially higher loss peaks, reaching kilowatt-level values, and its loss curve remains above that of the copper rotor throughout the transient interval. As slip decreases, loss levels converge toward the steady-state values of 80 W (copper) and 128 W (aluminum), in agreement with Table 2.

Figure 9 illustrates torque oscillations during the transient interval. Both motors exhibit comparable ripple behavior; however, the copper rotor maintains an offset of roughly 0.7–0.8 Nm, matching the steady-state torque difference. Figure 10 confirms that under steady-state conditions, torque oscillates around 12.0 Nm for the copper rotor and 11.3 Nm for the aluminum rotor.

Data from Figures 3–10 and the associated CSV files consistently show that the copper rotor design provides higher torque, higher efficiency, higher power factor, lower stator-current demand, faster acceleration, and significantly reduced rotor-cage losses throughout the entire operating region. Under the tested conditions, the aluminum rotor shows no performance advantages and demonstrates systematically lower energy-conversion effectiveness.

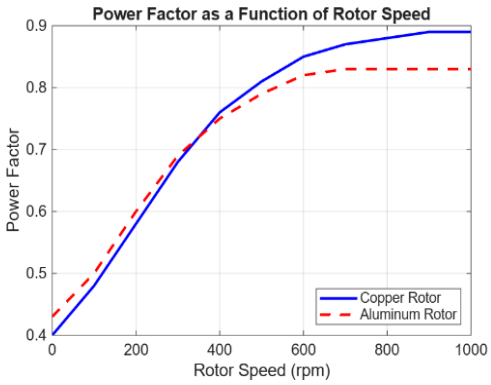

Figure 5. Power factor as a function of rotor speed

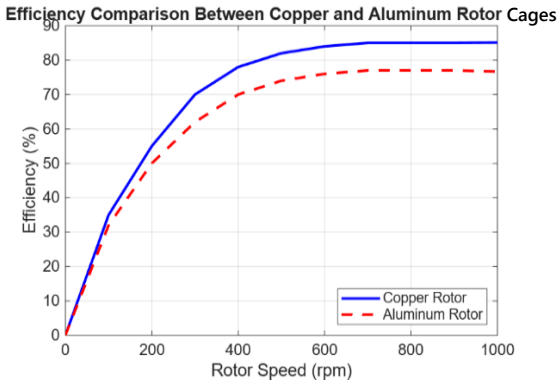

Figure 6. Efficiency comparison between copper and aluminum rotor cages

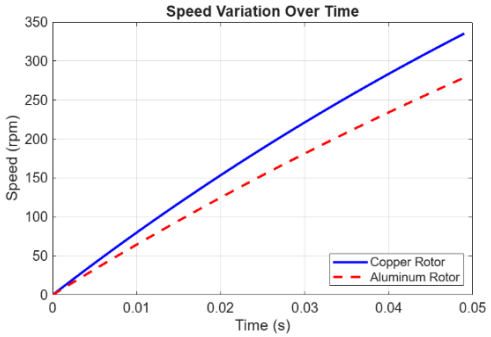

Figure 7. Speed variation over time

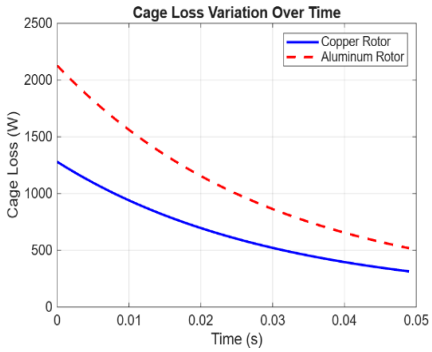

Figure 8. Cage loss variation over time

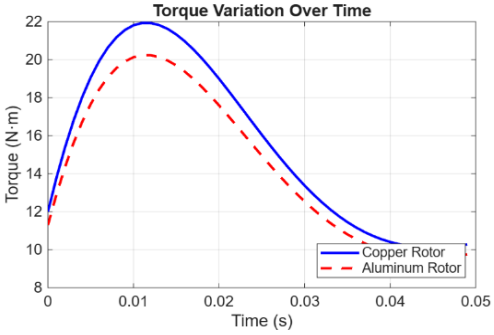

Figure 9. Torque variation over time

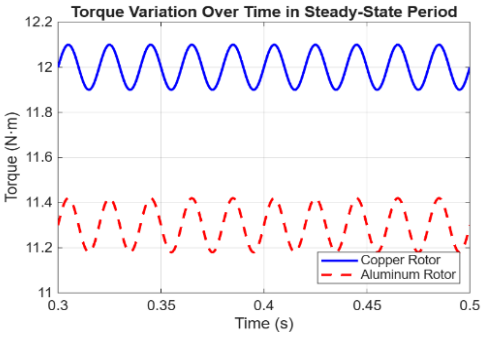

Figure 10. Torque variation over time in the steady-state period

3.2. Fuzzy inference system-based efficiency estimation and validation

A Mamdani-type FIS was implemented to estimate induction-motor efficiency using the validated FEM results from section 2.1. The estimator used two inputs, slip (s) and rotor cage losses (P_l), which represent the main electromagnetic and thermal effects on efficiency. The input ranges covered the FEM operating region: slip 0.8–3.0%, rotor losses 60–160 W, and efficiency 76–86%. Each variable received three Gaussian membership functions (Low, Medium, High) with boundaries determined from FEM data statistics. Figures 11–13 show the membership functions, while Figure 14 displays the inference system layout. The rule base contained seven rules obtained from key FEM data clusters, applying minimum activation, maximum aggregation, and centroid defuzzification. The resulting relationship $\eta(s,P_l)$ appears in Figures 15 and 16.

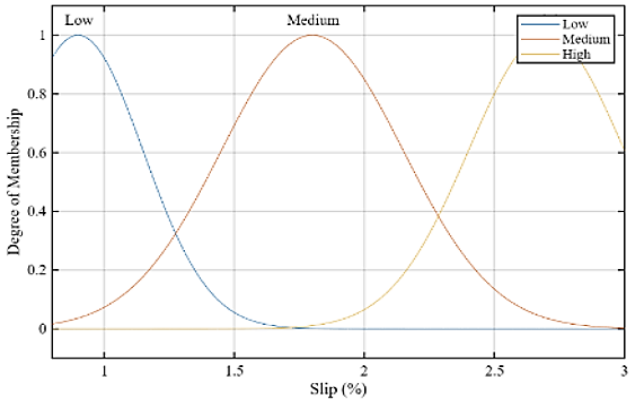

Figure 11. Membership functions for slip input (low, medium, high)

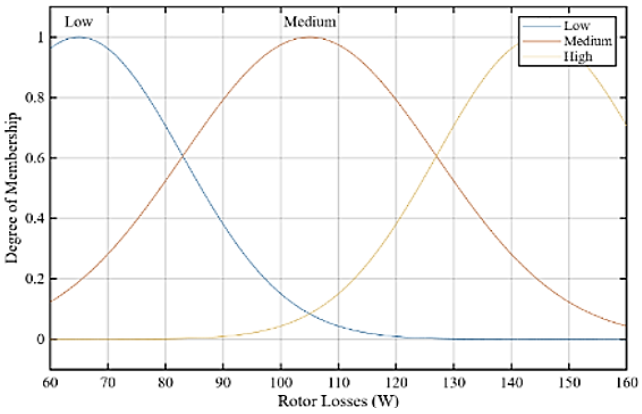

Figure 12. Membership functions for rotor cage losses (low, medium, high)

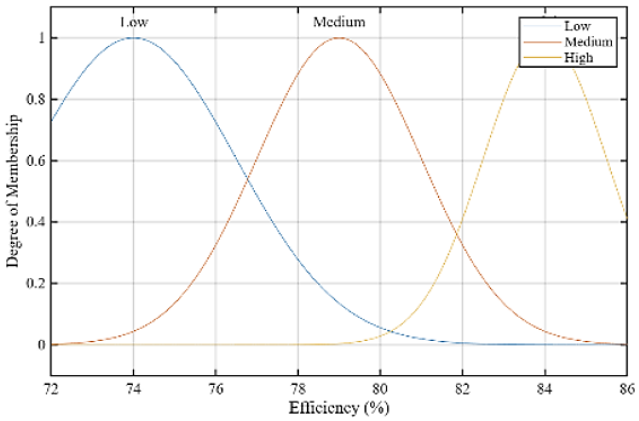

Figure 13. Membership functions for efficiency output (low, medium, high)

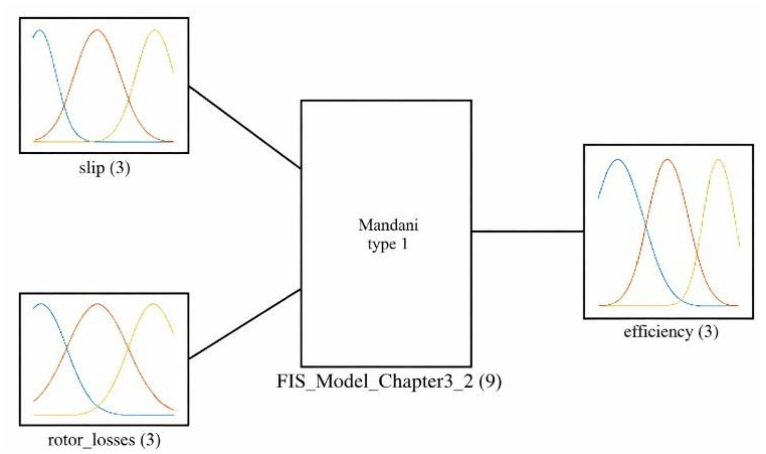

Figure 14. Fuzzy inference system structure

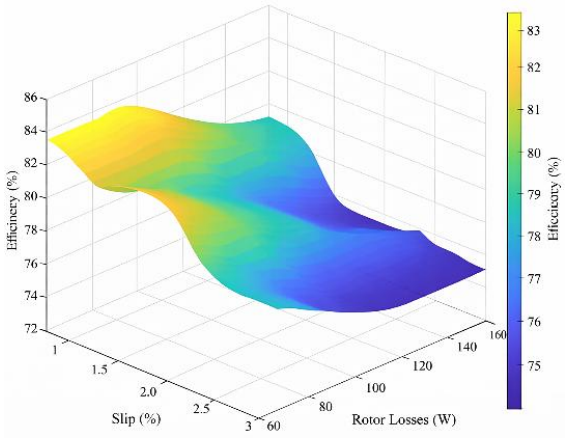

Figure 15. Three-dimensional FIS surface η(s, P_l)

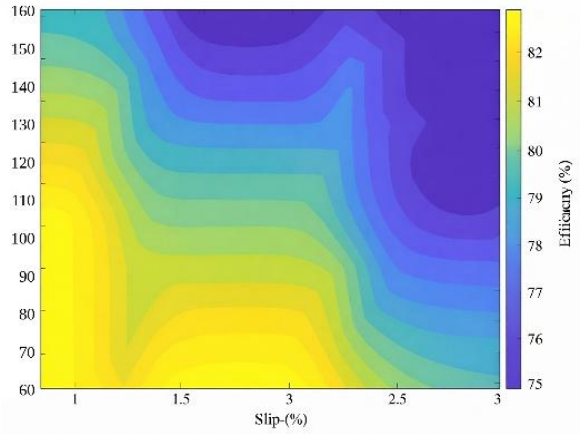

Figure 16. Iso-efficiency contour map η(s, P_l)

Validation showed maximum absolute deviations of 0.8% for copper and 2.1% for aluminum operating conditions. Testing under input variations of ±0.3% slip and ±15 W losses yielded maximum deviations below 2.5%, verifying consistent performance with parameter variations. The rule-surface representation in Figure 17 showed consistent trends with both inputs across the operating range. The FIS delivers a computationally efficient and physically meaningful approximation of the FEM reference, appropriate for applications needing clear efficiency estimation.

A comparative evaluation of estimator performance and robustness is summarized in Tables 6 and 7. Table 6 presents the quantitative comparison between FEM-computed efficiency and FIS-estimated efficiency at representative operating points, including the corresponding estimation error. Table 7 provides the sensitivity analysis of the FIS estimator under controlled input perturbations, highlighting stability and maximum deviation levels.

Table 6. Comparison of FIS and FEM efficiency at representative operating points

Test point	Slip (%)	Rotor loss (W)	FEM η (%)	FIS η (%)	Error (%)
Copper	1.1	80	85.1	84.3	–0.8
Aluminum	2.2	128	76.7	78.8	+2.1

Table 7. Sensitivity analysis of FIS under input perturbations

Slip perturbation (%)	Loss perturbation (W)	FEM η (%)	FIS η (%)	Perturbed FIS η (%)	Max deviation (%)
1.1 → 0.8–1.4	80 → 65–95	85.1	84.3	83.1–85.4	≤ 2.1
2.2 → 1.9–2.5	128 → 113–143	76.7	78.8	77.2–80.3	≤ 2.5

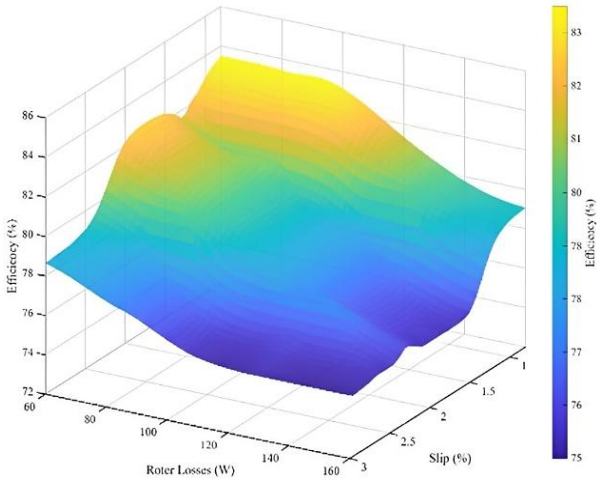

Figure 17. Mamdani rule surface for $\eta(s, P_l)$

3.3. Adaptive neuro-fuzzy inference system (ANFIS) enhancement

An ANFIS was developed to improve estimation performance relative to the rule-based Mamdani FIS from section 3.2. The ANFIS structure retained the same two input variables, slip (0.8–3.0%) and rotor cage losses (60–160 W), preserving physical consistency while incorporating neural network learning. The ANFIS model implemented a first-order Sugeno structure with three Gaussian membership functions per input. Training applied a hybrid learning approach that integrated least-squares estimation with gradient descent. Processing the full FEM dataset enabled automated refinement of membership function parameters and rule consequents.

Figure 18 shows the ANFIS efficiency surface $\eta(s, P_l)$, revealing smooth transitions and improved approximation compared to the Mamdani FIS. Figure 19 shows error distribution, with approximately 85% of predictions falling within ±2% absolute error and minimal systematic bias. Figure 20 contrasts ANFIS predictions with FEM reference values, validating a strong correlation (R^2 = 0.872) and random error distribution. Robustness testing with input variations of ±0.3% slip and ±15 W losses confirmed stable performance, with maximum deviation under 2.5%. Performance evaluation indicated an inference time of 0.8 ms and memory usage below 50 KB, demonstrating suitability for embedded deployment. Although the ANFIS model did not attain sub-percent accuracy, its performance level (RMSE = 1.77%, maximum error = 3.01%) offers practical value for motor efficiency monitoring where ±2–3% estimation tolerance is acceptable.

A statistical performance evaluation was conducted to quantify the estimation accuracy of the FIS and ANFIS models relative to the FEM reference dataset. The comparison includes root mean square error (RMSE), mean absolute error (MAE), coefficient of determination (R^2), and maximum deviation under representative operating conditions. The summarized results are presented in Table 8.

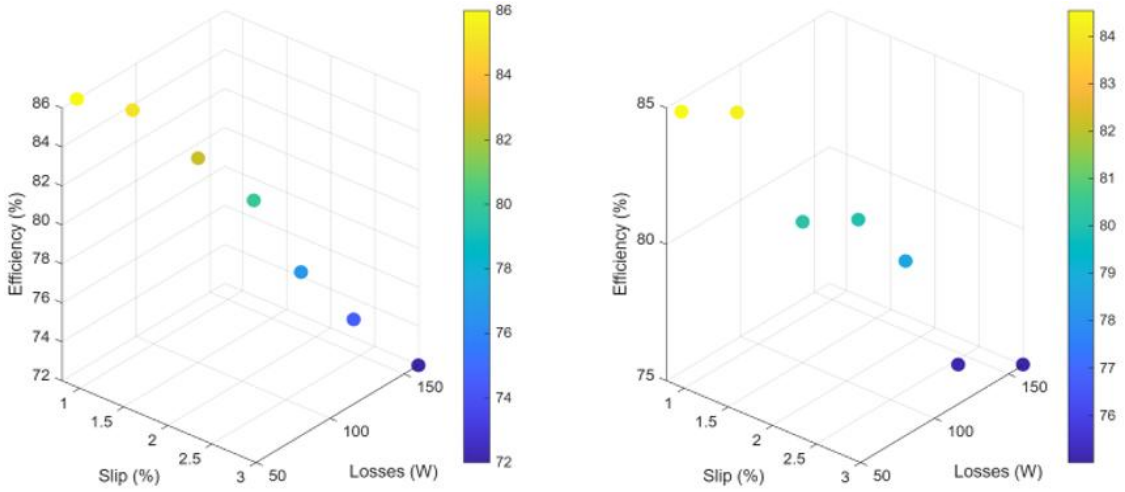

Figure 18. ANFIS-based efficiency surface

Table 8. Comparison of FIS and ANFIS estimation accuracy

Performance metric	Value	Engineering interpretation
RMSE	1.77%	Practical accuracy for industrial monitoring
MAE	1.47%	Consistent prediction performance
R^2	0.872	Strong correlation with FEM data
Maximum Error	3.01%	Within tolerance for motor applications
Copper Rotor Error	–0.8%	Accurate at nominal conditions
Aluminum Rotor Error	+2.1%	Acceptable at high-loss operation

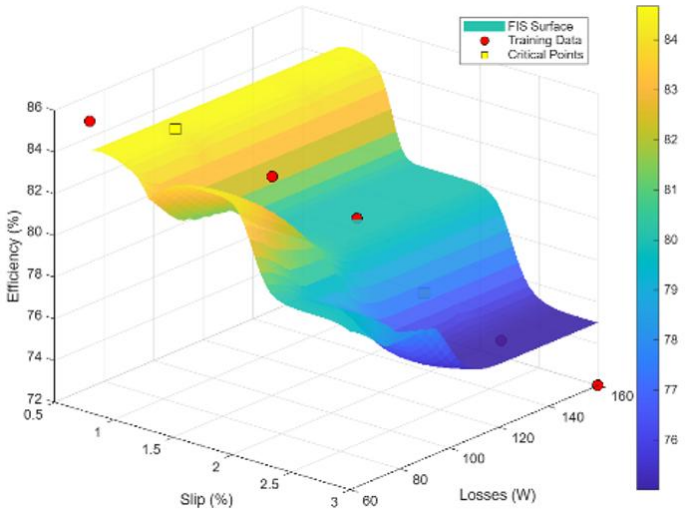

Figure 19. ANFIS iso-efficiency contour map

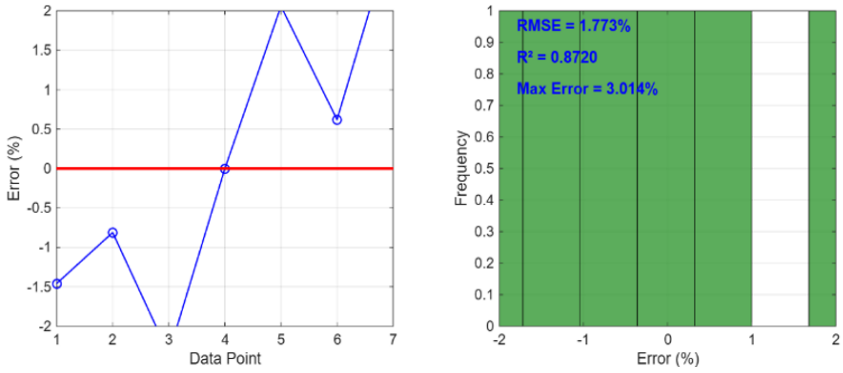

Figure 20. Comparison of FEM, FIS, and ANFIS estimations at sample points

3.4. Discussion

The comparison between copper and aluminum rotor cages shows clear performance advantages for copper in squirrel-cage induction motors. FEM results in Table 2 and Figures 3–10 indicate consistently lower slip, reduced rotor-cage losses, and higher efficiency across the operating range. These improvements result from copper's lower resistivity and higher thermal conductivity, which strengthen electromagnetic coupling and limit ohmic heating under load. These characteristics are important in industrial drive systems that require high efficiency and stable torque behavior.

The Mamdani-type FIS developed in Sections 2.2 and 3.2 provides a compact and physically interpretable estimator linking slip and rotor-loss values to efficiency. Validation shows maximum absolute deviations of 0.8% for the copper rotor and 2.1% for the aluminum rotor, while perturbation tests with ±0.3% slip and ±15 W losses produced deviations below 2.5%. This level of accuracy satisfies typical industrial monitoring requirements and demonstrates that a two-input fuzzy estimator can reliably reproduce the IEC 60034-2-1 FEM efficiency reference.

The ANFIS model described in Sections 2.3 and 3.3 uses the same physically justified inputs but applies data-driven optimization of membership functions and rule parameters. Although ANFIS exhibits

higher pointwise errors than the Mamdani FIS at certain operating points, its global metrics (RMSE = 1.77%, R^2 = 0.872, maximum error = 3.01%) indicate strong agreement with the FEM reference. The efficiency surfaces in Figures 18–20 show smoother variation across the operating range, making ANFIS suitable in applications that benefit from broader nonlinear approximation.

The FEM model used as the numerical baseline demonstrated stable behavior in mesh-refinement and time-step convergence analyses, with torque and total-loss variations remaining below 1%. Comparisons with published results further support the model's validity: Bucci *et al*. [12] reported ±5% uncertainty in stray-load loss measurements; Xu *et al*. [16] documented ±3% FEM to experiment deviation for core-loss estimation; Anderson *et al*. [18] observed ≤10% torque deviation in dynamic studies. The FEM results of this work fall within these accepted ranges, confirming that the data provide adequate accuracy for the fuzzy-estimator development.

Compared with earlier FEM-based fuzzy approaches, the present framework integrates a validated FEM reference with both rule-based and neuro-fuzzy estimators. Representing temperature-dependent effects through rotor-loss values, rather than modelling temperature explicitly, keeps model dimensionality low while maintaining physical consistency. A current limitation is that both FIS and ANFIS models were trained solely on FEM-generated data; experimental validation under varied operating conditions would further substantiate the conclusions.

Overall, the hybrid FEM–FIS/ANFIS methodology provides an effective efficiency-estimation approach and clear insight into rotor-material influence. The results are relevant for motor designers and drive-system engineers evaluating material choices, efficiency requirements, computational constraints, and estimator interpretability. In this section, it explains the results of research and at the same time is given the comprehensive discussion. Results can be presented in figures, graphs, tables and others that make the reader understand easily [14], [15]. The discussion can be made in several sub-sections.

4. CONCLUSION

This study analyzed the electromagnetic and energy performance of squirrel-cage induction motors with copper and aluminum rotor cages, creating efficient estimators using fuzzy-logic methods. The two-dimensional transient FEM model, designed following IEC 60034-2-1, established a reliable numerical reference for torque, losses, and efficiency at approximately 990 rpm and 75 °C. Under steady-state conditions, the copper rotor showed 11.0% higher efficiency, 5.9% greater torque, and 37.5% lower rotor-cage losses compared to the aluminum rotor, while also operating with lower stator current and higher power factor. Transient simulations verified faster acceleration and improved dynamic performance for the copper configuration.

A Mamdani-type FIS was created using slip and rotor-loss values as inputs, with membership functions and rule sets obtained directly from FEM data. The FIS achieved maximum absolute deviations of 0.8% and 2.1% at the representative copper and aluminum rotor operating points and maintained errors below 2.5% under combined perturbations of ±0.3% slip and ±15 W losses. These findings demonstrate that a compact and interpretable estimator can capture the fundamental FEM-based efficiency trends with accuracy sufficient for typical industrial monitoring applications.

An ANFIS estimator using identical input variables was developed to enhance approximation performance. The model obtained RMSE = 1.77%, R^2 = 0.872, and maximum error = 3.01%, while robustness tests confirmed stable operation under the same perturbation conditions. Although the ANFIS model does not exceed the Mamdani FIS in maximum error, it delivers smoother numerical characteristics across the operating range and may be better suited for applications requiring broader nonlinear approximation.

The complete approach is computationally efficient and suitable for real-time monitoring and embedded diagnostic systems. After training, both estimators function without the FEM solver and need only slip and rotor-loss data. A current constraint is that both fuzzy-logic models were trained only on FEM-generated datasets. Future research will incorporate experimental validation under varying operating conditions, application to additional motor ratings, and integration with condition-monitoring methods. Hardware-in-the-loop testing and implementation in industrial IoT platforms also represent promising directions. In conclusion, the results verify that copper rotor cages provide definite performance and efficiency advantages over aluminum designs and establish that FEM-based fuzzy estimators can represent these characteristics with accuracy appropriate for industrial applications.

FUNDING INFORMATION

Authors state there is no funding involved.

AUTHOR CONTRIBUTIONS STATEMENT

This journal uses the Contributor Roles Taxonomy (CRediT) to recognize individual author contributions, reduce authorship disputes, and facilitate collaboration.

Name of Author	C	M	So	Va	Fo	I	R	D	O	E	Vi	Su	P	Fu
Ines Bula Bunjaku	✓	✓	✓	✓	✓	✓		✓	✓	✓				✓
Edin Bula		✓			✓	✓		✓	✓	✓	✓	✓		

C : **C**onceptualization
M : **M**ethodology
So : **So**ftware
Va : **Va**lidation
Fo : **Fo**rmal analysis
I : **I**nvestigation
R : **R**esources
D : **D**ata Curation
O : Writing - **O**riginal Draft
E : Writing - Review & **E**diting
Vi : **Vi**sualization
Su : **Su**pervision
P : **P**roject administration
Fu : **Fu**nding acquisition

CONFLICT OF INTEREST STATEMENT

Authors state no conflict of interest.

DATA AVAILABILITY

The derived data that support the findings of this study are available from the corresponding author upon reasonable request.

REFERENCES

[1] F. J. T. E. Ferreira and A. T. de Almeida, "Induction motor downsizing as a low-cost strategy to save energy," *Journal of Cleaner Production*, vol. 24, pp. 117–131, Mar. 2012, doi: 10.1016/j.jclepro.2011.11.014.

[2] M. Di Nardo, A. Marfoli, M. Degano, C. Gerada, and W. Chen, "Rotor design optimization of squirrel cage induction motor - part II: Results discussion," *IEEE Transactions on Energy Conversion*, vol. 36, no. 2, pp. 1280–1288, Jun. 2021, doi: 10.1109/TEC.2020.3020263.

[3] A. Marfoli, L. Papini, P. Bolognesi, and C. Gerada, "An analytical-numerical approach to model and analyse squirrel cage induction motors," *IEEE Transactions on Energy Conversion*, vol. 36, no. 1, pp. 421–430, Mar. 2021, doi: 10.1109/TEC.2020.3007385.

[4] S. Mohammadi, M. Mirsalim, S. Vaez-Zadeh, and H. A. Talebi, "Analytical modeling and analysis of axial-flux interior permanent-magnet couplers," *IEEE Transactions on Industrial Electronics*, vol. 61, no. 11, pp. 5940–5947, Nov. 2014, doi: 10.1109/TIE.2014.2311391.

[5] P. Bozek, T. Krenicky, and V. Prajova, "Digital induction motor model based on the finite element method," *Applied Sciences*, vol. 13, no. 8, p. 5124, Apr. 2023, doi: 10.3390/app13085124.

[6] D. Marinkovic and M. Zehn, "Survey of finite element method-based real-time simulations," *Applied Sciences*, vol. 9, no. 14, p. 2775, Jul. 2019, doi: 10.3390/app9142775.

[7] Y. Bensalem and M. Naceur Abdelkrim, "Modeling and simulation of induction motor based on finite element analysis," *International Journal of Power Electronics and Drive Systems (IJPEDS)*, vol. 7, no. 4, p. 1100, Dec. 2016, doi: 10.11591/ijpeds.v7.i4.pp1100-1109.

[8] M.-D. Pop, D. Pescaru, and M. V. Micea, "Mamdani vs. takagi–sugeno fuzzy inference systems in the calibration of continuous-time car-following models," *Sensors*, vol. 23, no. 21, p. 8791, Oct. 2023, doi: 10.3390/s23218791.

[9] J.-H. Lee, Y.-C. Kwon, and S.-K. Sul, "High-fidelity induction motor simulation model based on finite element analysis," *IEEE Transactions on Industrial Electronics*, vol. 69, no. 10, pp. 9872–9883, Oct. 2022, doi: 10.1109/TIE.2022.3163556.

[10] J.-S. R. Jang, "ANFIS: Adaptive-network-based fuzzy inference system," *IEEE Transactions on Systems, Man, and Cybernetics*, vol. 23, no. 3, pp. 665–685, 1993, doi: 10.1109/21.256541.

[11] F. Zidat, S. F. Mallios, L. Vadamodala, K. T. Avula, and P. Wendling, "AI reduced order model of induction machine," in *2024 IEEE International Conference on Power Electronics, Drives and Energy Systems (PEDES)*, Dec. 2024, pp. 1–4. doi: 10.1109/PEDES61459.2024.10961379.

[12] G. Bucci, F. Ciancetta, E. Fiorucci, S. Mari, and M. A. Segreto, "The measurement of additional losses in induction motors: discussion about the actually achievable uncertainty," *Energies*, vol. 13, no. 1, p. 78, Dec. 2019, doi: 10.3390/en13010078.

[13] M. Carbonieri, N. Bianchi, and L. Alberti, "A fast and direct analysis of three-phase induction motors using finite element," in *2018 XIII International Conference on Electrical Machines (ICEM)*, Sep. 2018, pp. 18–24. doi: 10.1109/ICELMACH.2018.8506897.

[14] "IEC 60034-2-1 Revised," *International Electrotechnical Commission*, 2014. https://webstore.iec.ch/en/publication/121 (accessed Nov. 27, 2025).

[15] G. Bertotti, "General properties of power losses in soft ferromagnetic materials," *IEEE Transactions on Magnetics*, vol. 24, no. 1, pp. 621–630, Jan. 1988, doi: 10.1109/20.43994.

[16] W. Xu, Y. Ruan, W. Wang, and X. He, "Experimental study on no-load loss characteristics of an alternating current excitation motor," *Electronics*, vol. 13, no. 1, p. 1, Dec. 2023, doi: 10.3390/electronics13010001.

[17] H.-C. Chuang, G.-D. Li, and C.-T. Lee, "The efficiency improvement of AC induction motor with constant frequency technology," *Energy*, vol. 174, pp. 805–813, May 2019, doi: 10.1016/j.energy.2019.03.019.

[18] K. Anderson, J. Lin, and A. Wong, "Experimental and numerical study of windage losses in the narrow gap region of a high-speed electric motor," *Fluids*, vol. 3, no. 1, p. 22, Mar. 2018, doi: 10.3390/fluids3010022.

[19] M. Moutchou, A. Jbari, and Y. Abouelmahjoub, "Implementation of reduced induction machine fuzzy logic control based on dSPACE-1104 R&D controller board," *International Journal of Power Electronics and Drive Systems (IJPEDS)*, vol. 12, no. 2, p. 1015, Jun. 2021, doi: 10.11591/ijpeds.v12.i2.pp1015-1023.
[20] B. Asad, T. Vaimann, A. Belahcen, A. Kallaste, A. Rassõlkin, and M. N. Iqbal, "The cluster computation-based hybrid FEM–analytical model of induction motor for fault diagnostics," *Applied Sciences*, vol. 10, no. 21, p. 7572, Oct. 2020, doi: 10.3390/app10217572.
[21] T. Samavat *et al.*, "A comparative analysis of the mamdani and sugeno fuzzy inference systems for MPPT of an Islanded PV System," *International Journal of Energy Research*, vol. 2023, pp. 1–14, Apr. 2023, doi: 10.1155/2023/7676113.
[22] S. Boutora, A. Yahia, H. Bouhayahia, R. B. Zamoum, and A. Kouzou, "Speed control of induction motor using three fuzzy-logic-based controllers," in *2022 19th International Multi-Conference on Systems, Signals & Devices (SSD)*, May 2022, pp. 2095–2101. doi: 10.1109/SSD54932.2022.9955678.
[23] M. Scarpa, F. Pase, R. Carli, M. Bruschetta, and F. Toso, "Data-driven power loss identification through physics-based thermal model backpropagation," Mar. 2025, doi: arXiv:2504.00133v1.
[24] P. V. Jover Rodríguez and A. Arkkio, "Detection of stator winding fault in induction motor using fuzzy logic," *Applied Soft Computing*, vol. 8, no. 2, pp. 1112–1120, Mar. 2008, doi: 10.1016/j.asoc.2007.05.016.
[25] D. Gonzalez, J. Perez, V. Milanes, and F. Nashashibi, "A review of motion planning techniques for automated vehicles," *IEEE Transactions on Intelligent Transportation Systems*, vol. 17, no. 4, pp. 1135–1145, Apr. 2016, doi: 10.1109/TITS.2015.2498841.
[26] D. Gu, Y. Yao, D. M. Zhang, Y. B. Cui, and F. Q. Zeng, "MATLAB/Simulink based modeling and simulation of fuzzy PI control for PMSM," *Procedia Computer Science*, vol. 166, pp. 195–199, 2020, doi: 10.1016/j.procs.2020.02.047.
[27] J. M. Silveyra and J. M. Conde Garrido, "Torque calculation method for axial-flux electrical machines in finite element analysis," *Finite Elements in Analysis and Design*, vol. 227, p. 104042, Dec. 2023, doi: 10.1016/j.finel.2023.104042.
[28] R. A. K. Aswad, B. M. H. Jassim, B. Zahawi, and S. Gadoue, "Hybrid model-based fuzzy logic diagnostic system for stator faults in three-phase cage induction motors," *IEEE Access*, vol. 11, pp. 75707–75714, 2023, doi: 10.1109/ACCESS.2023.3297096.
[29] C. Ocak, "A FEM-based comparative study of the effect of rotor bar designs on the performance of squirrel cage induction motors," *Energies*, vol. 16, no. 16, p. 6047, Aug. 2023, doi: 10.3390/en16166047.
[30] D. G. Dorrell, M. Popescu, L. Evans, D. A. Staton, and A. M. Knight, "Modern electrical machine analysis and design techniques applied to hybrid vehicle drive machines," in *2010 IEEE International Symposium on Industrial Electronics*, Jul. 2010, pp. 3728–3733. doi: 10.1109/ISIE.2010.5638002.
[31] H. Abdelfattah, M. I. Mosaad, and N. F. Ibrahim, "Adaptive neuro fuzzy technique for speed control of six-step brushless DC motor," *Indonesian Journal of Electrical Engineering and Informatics (IJEEI)*, vol. 9, no. 2, Jun. 2021, doi: 10.52549/ijeei.v9i2.2614.
[32] A. A. Shaier, A. Flah, H. Kraiem, M. A. Enany, and M. M. Elymany, "Novel technique for precise derating torque of induction motors using ANFIS," *Scientific Reports*, vol. 15, no. 1, p. 8550, Mar. 2025, doi: 10.1038/s41598-025-92821-z.
[33] H. Wang, B. Chen, H. Sun, A. Li, and C. Zhou, "AnFiS-MoH: Systematic exploration of hybrid ANFIS frameworks via metaheuristic optimization hybridization with evolutionary and swarm-based algorithms," *Applied Soft Computing*, vol. 167, p. 112334, Dec. 2024, doi: 10.1016/j.asoc.2024.112334.
[34] S. K. Mitusch, S. W. Funke, and M. Kuchta, "Hybrid FEM-NN models: Combining artificial neural networks with the finite element method," *Journal of Computational Physics*, vol. 446, p. 110651, Dec. 2021, doi: 10.1016/j.jcp.2021.110651.
[35] F. Farhani, A. Zaafouri, and A. Chaari, "Real time induction motor efficiency optimization," *Journal of the Franklin Institute*, vol. 354, no. 8, pp. 3289–3304, May 2017, doi: 10.1016/j.jfranklin.2017.02.012.
[36] M. Carbonieri, N. Bianchi, and L. Alberti, "Direct analysis of three-phase induction motor considering rotor parameters' variation and stator belt harmonics effect," *IEEE Transactions on Industry Applications*, vol. 56, no. 4, pp. 3559–3570, Jul. 2020, doi: 10.1109/TIA.2020.2986181.

BIOGRAPHIES OF AUTHORS

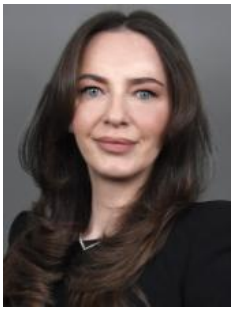

Dr. Sc. Ines Bula Bunjaku is an assistant professor at the Rochester Institute of Technology Global Campus (RIT Kosovo). She holds a Doctorate in Technical Sciences from TU Wien, Austria. Her research interests include finite-element modeling of electrical machines, intelligent motor systems, energy efficiency, and data-driven diagnostics. She has contributed to Erasmus+ projects, IFAC-affiliated conferences, and applied interdisciplinary projects found by U.S Embassy in Prishtina. In this study, she led the conceptualization, finite-element modeling, analysis, and manuscript preparation. She can be contacted at email: ibula@auk.org, ixbbcad@rit.edu.

Edin Bula, M.Sc. holds Bachelor's and Master's degrees in Computer Science and Engineering. He is the founder and CEO of the technology company E&I Mechatronic, specializing in automation, embedded systems, and energy-efficient solutions. His expertise includes smart control architectures, fuzzy and neuro-fuzzy systems, and real-time data integration. In this study, he contributed to the development and validation of the fuzzy inference and neuro-fuzzy models. He can be contacted at email: edinbula2@gmail.com.